INTERNATIONAL JOURNAL OF HYDROGEN ENERGY 37 (2012) 14801–14811

Available online at www.sciencedirect.com

SciVerse ScienceDirect

journal homepage: www.elsevier.com/locate/he

Plant-wide control design for fuel processor system with PEMFC

L. Nieto Degliuomini [a,b,1], D. Zumoffen [a,b], M. Basualdo [a,b,*,1]

[a] Computer Aided for Process Engineering Group (CAPEG). French-Argentine International Center for Information and Systems Sciences, (CIFASIS-CONICET-UNR-UPCAM), 27 de Febrero 210 bis, S2000EZP Rosario, Argentina

[b] Universidad Tecnológica Nacional – FRRo, Zeballos 1341, S2000BQA, Rosario, Argentina

ARTICLE INFO

Article history:
Received 8 September 2011
Received in revised form
3 January 2012
Accepted 31 January 2012
Available online 2 March 2012

Keywords:
Bio-ethanol processor
Fuel cell
Control structure design
Hydrogen production

ABSTRACT

The main contribution of this work is the application of a novel technique for the plant-wide control design to a challenging bio-ethanol processor system for hydrogen production. It is based on steam reforming, followed by high and low-temperature shift reactors and preferential oxidation. The obtained hydrogen feeds a fuel cell for automotive use. The control structure is defined by using a well-tested, systematic and generalized procedure, named minimum square deviation. It allows keeping the process at the operating point of maximum efficiency. This design procedure accounts both, set point as well as disturbances effects which can be sorted according to their importance through specific weighting matrices. The first step of this approach solves the problem of obtaining the best-controlled variables. Then, the search involves testing several combinations between the available input–output variables. The overall processor system with fuel cell, able for doing the tests, was modeled by using mass and energy balances, chemical equilibrium, thermodynamic models and feasible heat transfer conditions. The selected control structure is rigorously tested applied in the dynamic model of the complete plant. The computational implementation of this model was made by using a suitable integration of three well-known programs: MATLAB, HYSYS and ADVISOR. The simulations are performed for hybrid vehicle (PEMFC and supercapacitors). The disturbance profile corresponds to a urban standard driving cycle, which is one of the most exigent. The conclusions are based on fuel consumptions, typical performance indexes used for control strategy evaluations and a trade-off between cost investments and efficiency.

1. Introduction

The liquid fuel conversion into useful power in the context of the automobile industry reports its maximum efficiency for the internal combustion engines of around 35%. In the last decades the alternative use of the Fuel Cells (FCs) has been growing up specially because they can achieve up to 83% of global efficiency [1]. The main reason for this difference is that

* *Corresponding author*. Computer Aided for Process Engineering Group (CAPEG). French-Argentine International Center for Information and Systems Sciences, (CIFASIS-CONICET-UNR-UPCAM), 27 de Febrero 210 bis, S2000EZP Rosario, Argentina. Tel.: +54 341 4237248 304; fax: +54 341 482 1772.

E-mail addresses: nieto@cifasis-conicet.gov.ar (L. Nieto Degliuomini), zumoffen@cifasis-conicet.gov.ar (D. Zumoffen), basualdo@cifasis-conicet.gov.ar (M. Basualdo).

[1] Tel.: +54 341 4237248 304; fax: +54 341 482 1772.

0360-3199/$ – see front matter
doi:10.1016/j.ijhydene.2012.01.169

FCs do not have mobile parts so, the energy losses because of friction effects are avoided.

The FCs are good alternatives to the internal combustion engines mainly because they are more efficient and can be completely fueled with renewable sources. Particularly, Proton Exchange Membrane Fuel Cells (PEMFCs), require hydrogen to produce electricity. However, the hydrogen storage and transportation are risky. In this context, an onboard processing system to produce H_2 from renewable materials, such as bio-ethanol represents a valuable option. This bio-fuel is relatively easy and cheap to produce and can be obtained from agricultural or sugar industry residues. Gregorini et al. [2] analyzed the conditions for Argentine. They focused on reducing the price of this alternative energy source to be economically competitive with fossil fuels. By this way, the produced CO_2 during the reforming stage will be reabsorbed by crops growth for the following reaps, presenting a nearly closed carbon loop without net greenhouse gases emissions.

The primary methods used in reforming hydrocarbons to produce hydrogen for use in PEM fuel cells are Ethanol Steam Reforming (ESR), Partial Oxidation, and a combination of both called auto-thermal reforming. ESR is considered in this work mainly because of its ability to produce higher H_2 molar fractions. Some specific issues of this process are accounted to formulate the control structure. Hence, since the reaction scheme is endothermic it needs an auxiliary combustion reactor to fulfill the thermal requirements of the ESR reactor. Carbon monoxide (CO) is one of the byproducts of the reforming reaction. It must be kept at a very low concentration of the produced hydrogen that feeds the Fuel Cell because its membrane is sensitive to be poisoned by CO. Additionally, the heat integration must be considered to improve the efficiency of the hydrogen production via bio-ethanol. Some interesting ideas about a heat exchangers network design, able to guarantee maximum heat recovery and provide the best efficiency, was recently presented in [3].

The goal of this work is to design a proper control structure able to keep the overall system at the wanted operating point of highest efficiency despite disturbances. The need of using a systematic approach for the plant-wide control designs is based on the fact that, an apparently appropriate control scheme for isolated unit operations may actually lead to an inoperable plant when they are connected. Particularly, when the process has recycle streams and energy integration the interaction effect could be very important. The process synthesis stage generally defines several control objectives such as product quality, product rate, active constraints, etc. The selected plant-wide control structure must guarantee stability for the closed loop system. In addition, the investment cost is involved too, since it is related to the number of sensors, actuators, controllers to be installed and the final dynamic control performance.

An important number of process control researchers have developed many systematic plant-wide control methodologies and applied them to chemical processes. It is remarkable that, in the majority of the works, they use the relative gain array (RGA) based techniques for control loop configuration. RGA was defined in the pioneering work of Bristol [4]. Even though it is well known and has widespread industry applications, some limitations were recognized. Based on these, several new extensions of the RGA have appeared in the literature. Particularly, in this work, the non-square relative gain array (NRG), introduced by Chang and Yu [5], the generalized relative disturbance gain (GRDG) presented in Chang and Yu [6] and the recently developed relative normalized gain array (RNGA) by He et al. [7], together with the RGA have been considered in the approach used here. In this work, the objective function to be minimized for defining the controlled variables (CVs) is the sum of the square deviations in steady state of the uncontrolled output variables (SSD_{yr}). The optimal solution can be found by the use of genetic algorithm (GA) independently of the problem dimension. The methodology implemented in the fuel processor system and fuel cell given here, allows to configure the loops pairing by considering the trade-off between the need of changing operating points (servo) and the rejection of some critical disturbances (good regulator behavior). It can be done thanks to the definition of a proper function, named net load effect, containing both set point and perturbation effects. The relative importance between them is handled through specific weighting parameters. For selecting the best pairs between CVs and the manipulated variables (MVs) the minimization of the net load effect is done subjected to find a proper plant model, in the context of Internal Model Control design.

The methodology applied in this work integrates and extends the results for plant-wide control which has been tested previously, by the group of Basualdo, in several academic cases of study [8–10]. Then, they give confidence on provide promising results on this challenging and novel process. Hence, after the plant-wide control design is done, is tested dynamically to verify if the main process objectives and operational conditions are satisfied. Finally, a set of simulation results and conclusions are included to remark the main contributions of this proposal.

2. Plant-wide control approach description

The generalized procedure for plant-wide control, called minimum square deviation (MSD), is introduced in this section. The main stages of the algorithm are schematically shown in Fig. 1. In this block diagram a direct connection with process synthesis is assumed, it allows to perform an intensive interchange of information, and by successive iterations a controllable process is achievable. Simultaneously, the main control objectives, determined in the synthesis stage, can be effectively incorporated within this methodology.

2.1. *Initial step*

All industrial processes are pointed towards obtaining the highest possible benefits. Process operation must be optimized accounting economic objectives. This procedure allows to obtain valuable information regarding which variables should be controlled aiming this objective. As a first recommendation those variables found in their active constraints (equalities or inequalities) are suggested to be controlled. Optimization results can only be guaranteed within that operating point.

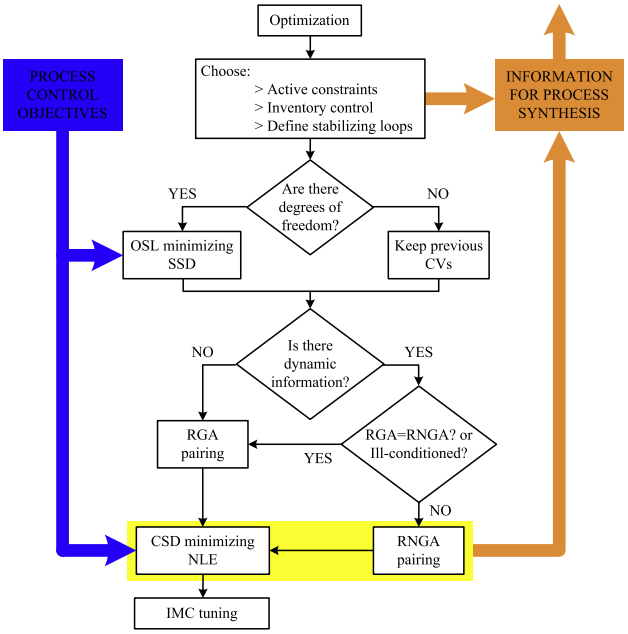

Fig. 1 – Minimum square deviation (MSD) procedure for plant-wide control.

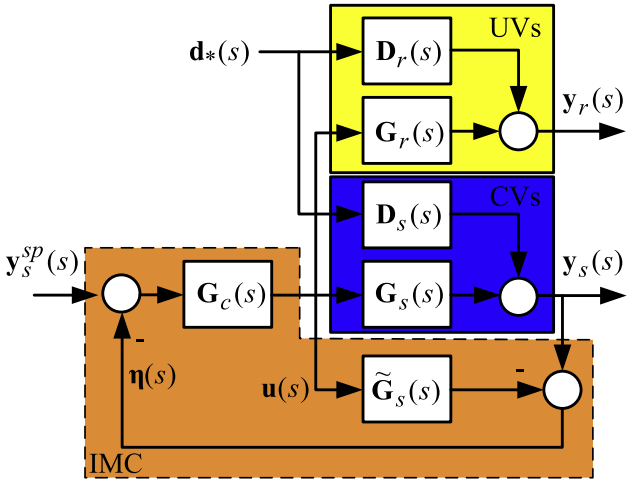

Fig. 2 – Generalized IMC structure.

Industrial processes could present unstable behavior in open loop operation. Then, it is necessary to stabilize the plant defining the minimal number of control loops needed. These loops include, for instance, pressure control in vessels, given the pure integrative nature of its behavior. The starting point of the proposed strategy is to define these loops. The works of [11] and [12] can be mentioned as examples on how to define them.

With the process stabilized, the system identification stage, using different strategies, can be done in order to obtain dynamic information of the plant. This reduced dynamic model is very useful for supporting the controllers tuning stage, the control structure selection via RNGA and the uncertainty analysis.

2.2. *Measurements selection*

If additional variables can be controlled by those manipulated variables which have not been used yet must be considered after finishing the previous stage. In this case, the issue is to determine which variables must be selected to achieve a specific goal. To solve this problem the well-known control structure, named Internal Model Control (IMC), presented in Fig. 2, is useful for giving support for the calculations. $\mathbf{G}(s) = [\mathbf{G}_s(s)^T, \mathbf{G}_r(s)^T]^T$ represents the transfer function matrix (TFM) of the process with n inputs and m outputs, being $m > n$,

$$\mathbf{y}(s) = \mathbf{G}(s)\mathbf{u}(s) + \mathbf{D}(s)\mathbf{d}_*(s) \tag{1}$$

where $\mathbf{D}(s) = [\mathbf{D}_s(s)^T, \mathbf{D}_r(s)^T]^T$ is the TFM corresponding to the effect of output disturbances with dimension $m \times p$; $\mathbf{y}(s)$, $\mathbf{u}(s)$ and $\mathbf{d}_*(s)$ are output, input, and disturbance vectors with dimension $m \times 1$, $n \times 1$ and $p \times 1$ respectively.

The process is divided in two parts: one square, $\mathbf{G}_s(s)$, that includes the n output variables to be controlled and the other not necessarily square, $\mathbf{G}_r(s)$ that contains the $m - n$ uncontrolled variables. So, the process can be rewritten as

$$\mathbf{y}_s(s) = \mathbf{G}_s(s)\mathbf{u}(s) + \mathbf{D}_s(s)\mathbf{d}_*(s) \tag{2}$$

$$\mathbf{y}_r(s) = \mathbf{G}_r(s)\mathbf{u}(s) + \mathbf{D}_r(s)\mathbf{d}_*(s) \tag{3}$$

where $\mathbf{G}_s(s)$, $\mathbf{D}_s(s)$, $\mathbf{G}_r(s)$ and $\mathbf{D}_r(s)$ are the TFM of $n \times n$, $n \times p$, $(m-n) \times n$ and $(m-n) \times p$ respectively. Being $\tilde{\mathbf{G}}_s(s)$ an approximated model of $\mathbf{G}_s(s)$.

The problem can be parameterized to a particular CVs selection. In the context of Genetic Algorithms, $\mathbf{C}_i = [c_1, \ldots, c_m]$ belongs to a binary alphabet and parameterizes all the potential measurement points (sensors locations). $c_j = 1$ indicates that a sensor in the location j is needed and $c_j = 0$ the opposite situation. The combinatorial problem of Eq. (4) can be stated considering perfect control in steady state. It represents the minimizations of the deviations of y_r (in minimum square sense) respect to its operating conditions, when set point changes and individual disturbances occur.

$$\min_{C_i} \ \mathrm{SSE}_{y_r}(\mathbf{C}_i) = \min_{C_i} \left[\left\| \Lambda_2 \mathbf{S}_{sp}(\mathbf{C}_i) \Lambda_1 \right\|_F^2 + \left\| \Theta_2 \mathbf{S}_d(\mathbf{C}_i) \Theta_1 \right\|_F^2 \right] \tag{4}$$

subject to

$$\det(\mathbf{G}_s(\mathbf{C}_i)) \neq 0 \tag{5}$$

where Λ_1 and Λ_2 are diagonal matrices that allow to incorporate relative weights according to the amplitude in the references and the relative importance between the considered outputs. Θ_1 and Θ_2 play the same role as Λ_1 and Λ_2 but for disturbances. $\mathbf{S}_{sp} = [\mathbf{G}_r\mathbf{G}_s^{-1}]$ and $\mathbf{S}_d = [\mathbf{D}_r - \mathbf{G}_r\mathbf{G}_s^{-1}\mathbf{D}_s]$ are respectively the deviations of the uncontrolled variables for set point changes and disturbances. The constraint in (5) guarantees that the optimal solution for (4) is also a feasible one. Based on the block diagram of Fig. 2 it can be observed that the optimal solution $\mathbf{C}_i$, parameterizes $\mathbf{G}_s$ and this particular selection of the CVs eventually affects the feasibility of the future IMC control design. A more detailed explanation together with the associated properties are given in [10].

2.3. Control structure definition

There are no more degrees of freedom once the previous stage is finalized, as is shown in Fig. 1. Meaning, the n CVs were selected from the set of m potential measurement points. This selection was performed by minimizing the SSE_{yr} index via optimization. When the stabilization stage uses all the process degrees of freedom the optimization presented in the Section 2.2 is avoided. In both cases the new problem is to decide the input–output pairing, $n \times n$, and the controller structure. It could be decentralized (diagonal), full or sparse configuration.

Considering Fig. 2, the IMC theory and plant-model mismatch it can be defined

$$\mathbf{y}_s^{net}(s) = \mathbf{A}(s)\mathbf{y}_s^{sp}(s) + \mathbf{B}(s)\mathbf{d}_*(s) \tag{6}$$

being $\mathbf{y}_s^{net}(s)$ the net load which affects the CVs during the transient response. Working in steady state and accounting that $\mathbf{G}_c = \tilde{\mathbf{G}}_s^{-1}$,

$$\mathbf{A} = \mathbf{I} - \tilde{\mathbf{G}}_s\mathbf{G}_s^{-1} \tag{7}$$

$$\mathbf{B} = \tilde{\mathbf{G}}_s\mathbf{G}_s^{-1}\mathbf{D}_s \tag{8}$$

$$\tilde{\mathbf{G}}_{s\Gamma} = \mathbf{G}_s \otimes \Gamma, \quad \text{with} \quad \Gamma = \begin{bmatrix} \gamma_{11} & \cdots & \gamma_{1n} \\ \vdots & \ddots & \vdots \\ \gamma_{n1} & \cdots & \gamma_{nn} \end{bmatrix} \tag{9}$$

where $\otimes$ is the element-by-element product and Γ is a binary matrix with dimension $n \times n$, allows to select a specific model structure that minimizes the net load evaluation, NLE(Γ), in a sum of square deviation (SSD) sense, Thus, the new combinatorial problem can be stated as

$$\min_{\Gamma} \mathrm{NLE}(\Gamma) = \min_{\Gamma}\left[\left\|\Delta_1\mathbf{A}_\Gamma\Delta_2\right\|_F^2 + \left\|\Xi_1\mathbf{B}_\Gamma\Xi_2\right\|_F^2\right] \tag{10}$$

subject to

$$\mathbf{A}_\Gamma = \mathbf{I} - \tilde{\mathbf{G}}_{s\Gamma}\mathbf{G}_s^{-1} \tag{11}$$

$$\mathbf{B}_\Gamma = \tilde{\mathbf{G}}_{s\Gamma}\mathbf{G}_s^{-1}\mathbf{D}_s \tag{12}$$

$$\mathrm{Re}\left[\lambda_i\left(\mathbf{G}_s\tilde{\mathbf{G}}_{s\Gamma}^{-1}\right)\right] > 0, \quad i = 1, \ldots, n \tag{13}$$

where Δ_1, Δ_2, Ξ_1 and Ξ_2 are matrices that allow to incorporate the relative importance of both, set points and disturbance changes and, on the other hand, sort the outputs according to the plant objectives. The conditions stated in (11) and (12) allow to compute both $\mathbf{A}_\Gamma$ and $\mathbf{B}_\Gamma$ matrices from a particular model parametrization $\tilde{\mathbf{G}}_{s\Gamma}$. The constraint in (11) allows to check the stability condition in steady state for the current control structure, in the context of IMC [13]. Where $\lambda_i(\mathbf{G}_s\tilde{\mathbf{G}}_{s\Gamma}^{-1})$ is the i eigenvalue of the matrix $\mathbf{G}_s\tilde{\mathbf{G}}_{s\Gamma}^{-1}$ and Re[·] the real part function. There are several stability and robustness tests in the literature, either for steady state [14,15] and dynamic [16,17] analysis. Note that the final control structure depends on the selected model parametrization, $\mathbf{G}_c(s) = \tilde{\mathbf{G}}_{s\Gamma}^{-1}(s)\mathbf{F}(s)$. In [10] a deep study on this topic is presented.

3. Control structure design for the BPS with PEMFC

In this section, the main details about the MSD strategy implementation for plant-wide control design to the integrated bio-ethanol processor system (BPS) with PEM fuel cell is given.

3.1. Process description

The fuel processor system can be seen in Fig. 5. It consists of a Bio-Ethanol Steam Reforming plug flow reactor, where most of the conversion of ethanol to H_2 is made. Carbon monoxide which poisons the fuel cell catalyst is produced in the ESR, so additional processing is needed to remove this substance. There are three reactors that configure the cleaning system; these are two Water Gas Shift (WGS), one of high temperature (fast) and the other of low temperature, that favors the equilibrium of the reaction to higher conversion rates of CO. The third is a Preferential Oxidation of Carbon monoxide (CO-PrOx) reactor, where oxidation of CO into CO_2 is made; also, the undesired oxidation of H_2 occurs, so the catalyst is selected to improve the conversion of CO. Further details on the dynamic modeling, process constraints and normal behavior can be seen in [18].

3.1.1. Improvements on the FC efficiency

In order to integrate the Fuel Processor and Fuel Cell System with an entire vehicle and the energy management strategy, the detailed model developed in ADVISOR is used [19]. The FC and the strategy originally presented are replaced by the one

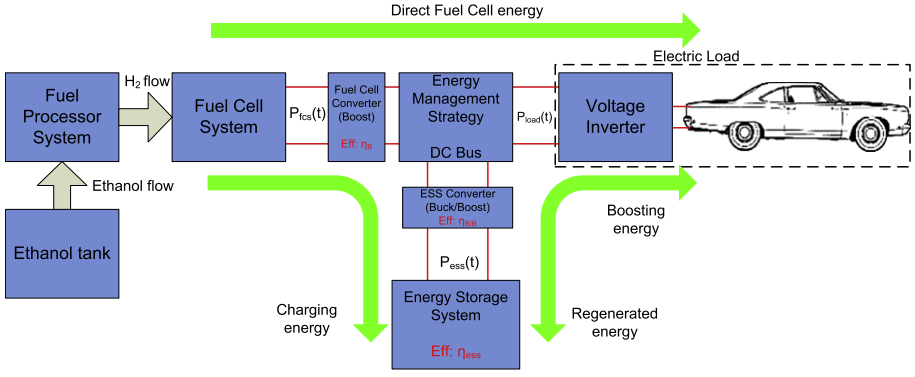

Fig. 3 – Configuration of the entire vehicle.

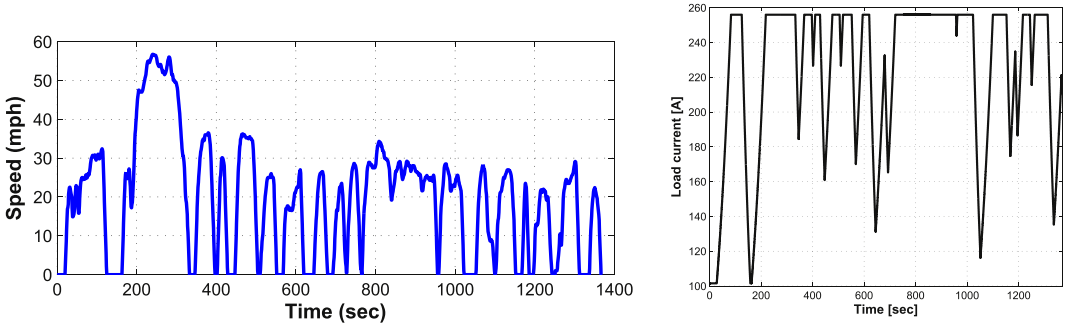

a UDDS speed profile

b Load stack current profile - Disturbance

Fig. 4 – Speed and current profile.

discussed in Section 3.2. The integrated power train along with the energy flows is shown in Fig. 3.

To evaluate the performance of a given hybrid vehicle, standard driving cycles are widely utilized in the literature. They represent urban and highway scenarios and were originally stated for measuring pollutant emissions and fuel economy of engines (DieselNet. Emission test cycles. Online, 2005). In Fig. 4(a) the speed demand corresponding to the Urban Dynamometer Driving Schedule (UDDS) is plotted. As can be seen, high power requirements take place during a relatively short fraction of time. If there is no energy storage, the FC must meet the highest peak power and, therefore, the FC is oversized most of the time. In addition, the efficiency of an FC is strongly degraded at low powers. Thus, if no hybridization is present, the FC has to work in large periods of time at a low efficiency zone. On the contrary, with an additional power source and a suitable energy management strategy it is possible to avoid these unfavorable operating zones. In a fuel cell hybrid system it is possible to boost the FC supplying energy to the load from the energy storage system. This energy was previously charged from the FC or regenerated from the load, e.g., from regenerative braking in automotive applications.

3.2. *Policy for maximizing the energy resource of the BPS with PEMFC*

In this work, the same policy for energy management given in detail in [20] is used. It is based on the Fuel Cell System efficiency map and it operates the FC preferably in its point of maximum efficiency in order to improve the hydrogen economy, although the final operating point of the FC is determined based on the actual power demand and the state of energy (SoE) of the Energy Storage System (ESS).

For safety reasons, the SoE first determines the working zone. If the SoE is too low, the FC operates at maximum power, supplying the required energy to the vehicle, and using the remaining to recharge the capacitors. If the SoE is too high, then the FC operates at minimum power allowing the capacitors to deplete giving the energy to the system.

When the system operates normally, the demand determines the operating zone. When the power demand is near the maximum efficiency point of the FC, it is set at that point, and using the energy from the ESS to fulfill the requirements of the system (charging or discharging). At high demand, the FC operates in load tracking mode, and above the maximum power of the FC, it operates at the upper bound, using the ESS to supply the remaining power. When the demand is low, the FC operates at minimum power, and the remaining energy is used to recharge the capacitors.

The FC operating point is determined as a function of the SoE(k) and the load power $P_{load}(k)$ (nomenclature is explained in Table 1). The transition between operating points is performed according to the constraints concerning the maximum fall power rate and the maximum power rate. Additionally, if $P_{load}(k) = 0, \quad \forall t \in [k1, k2]$ with $(k2 - k1) > T_{off}$, and, $SoE(k) > SoE_{hi}$ with $k > k2$, then, the FC is turned off to avoid unnecessary hydrogen consumption because the parasitic losses in the FC.

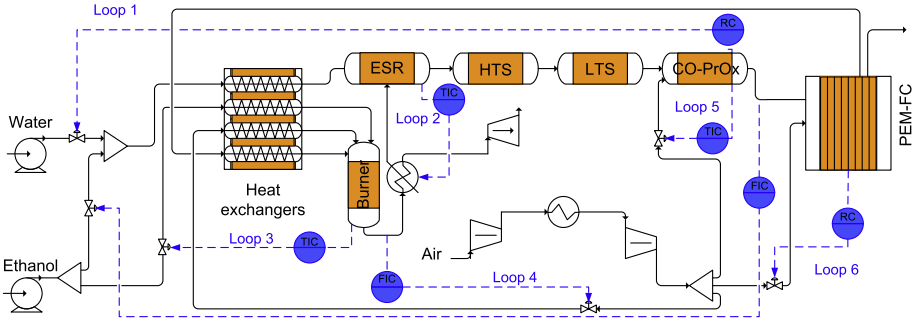

Fig. 5 – Plant-wide control of BPS + FC.

Table 1 – Nomenclature utilized.

Symbol	Description	Value
k	Current time	Seconds
$P_{fcs,lo}$	Lower net power	4000 W
$P_{fcs,hi}$	Higher net power	8000 W
P_{load}	Demanded Power	W
P_{fcs}	FC net power	W
P_{ess}	ESS output power	W
$P_{fcs,max}$	Maximum net power	10,000 W
$P_{fcs,maxeff}$	Maximum efficiency net power	8000 W
η_B	FC converter efficiency	0.95
$\eta_{B/B}$	ESS converter efficiency	0.95
η_{ess}	ESS efficiency	0.95
SoE_{lo}	Lower SoE	0.4
SoE_{hi}	Higher SoE	0.8
SoE_{min}	Mimimum SoE	0.3
SoE_{max}	Maximum SoE	0.9
T_{off}	Time to turn off FC	60 s

3.3. *Dynamic simulation results with the controlled BPS*

The control objectives of the BPS are to maintain adequate H_2 levels on the anode of the FC, because starvation can cause permanent damage and overfeeding will lead to hydrogen waste; the carbon monoxide levels of the anode inlet stream must be under 10 ppm and keeping the temperatures of the reactors set and FC at their operational range prevent damages and maintain the system efficiency. Table 2 lists the set of available variables in the BPS.

The first step of the methodology (see Fig. 1) is to achieve the plant stabilization. The primary control loops needed to stabilize the process are the pressure control of each reactor manipulating their corresponding exit flow, and the H_2 production to feed the fuel cell, determined by the current demand, with the fresh ethanol flow entering to the bio-ethanol steam reforming. Perfect control is assumed for the pressures and the H_2 control loop was adjusted via IMC theory [21]. Table 2 indicates these five stabilizing control loops with (*).

With the stabilized process, following the steps of the MSD strategy, a simplified model must be obtained by using system identification (SI) procedures. This technique allows to obtain a steady state and a dynamic linearized model of the process for control design purposes. According to Table 2, a model with 14 outputs (y_1–y_{14}), 6 available manipulated inputs (u_1–u_6) and 2 disturbances (d_1 and d_2) was obtained.

Next, it is necessary to define the controlled variables which are directly related to the measurements, because some degrees of freedom are still available. Six controlled variables must be selected from 14 available measurements via the SSD approach defined in Section 2.2. The optimal controlled variables selection is the result of a combinatorial problem since it should be chosen among the total amount of $14!/(6!(14-6)!) = 3003$ possible combinations. An exhaustive search can be implemented without computational problems.

The problem stated in Eqs. (4) and (5) is solved exhaustively with weight matrices $\Lambda_1 = \mathbf{I}_6$, $\Lambda_2 = \mathbf{I}_8$, $\Theta_1 = \mathbf{I}_2$ and $\Theta_2 = \mathbf{I}_8$, the best set of measurements that indicates the sensor location $\mathbf{C}_i$ can be found. The best first five solutions are displayed in Table 3, $\mathbf{C}_1$–$\mathbf{C}_5$, sorted by the SSD index. $\mathbf{I}_i$ is the identity matrix with dimension $i \times i$, and the parametrization $\mathbf{C}_i = [c_1, \ldots, c_m]$, which belongs to a binary alphabet, represents all the potential measurement points (sensor locations). $c_j = 1$ indicates that a sensor in the location j is needed and $c_j = 0$ the opposite situation, with $j = 1, \ldots, 14$. The best solution called $\mathbf{C}_1$ in Table 3 suggests that the controlled variables should be

- y_1: ESR exit temperature
- y_3: Burner exit temperature
- y_8: CO-PrOx exit temperature
- y_9: CO-PrOx molar ratio O_2/CO

Table 2 – Variables in the BPS + FC process.

Measured		Manipulated		Disturbances	
y_1	ESR exit temperature	u_1	Water to ESR inlet	d_1	Ethanol purity
y_2	Jacket exit gases temperature	u_2	Exchanged heat Q	d_2	Stack current
y_3	Burner exit temperature	u_3	Ethanol to Burner		
y_4	Burner entering molar flow	u_4	Oxygen to Burner		
y_5	Molar ratio H_2O/Ethanol	u_5	Oxygen to CO-PrOx		
y_6	HTS exit temperature	u_6	CM voltage		
y_7	LTS exit temperature	u_7	ESR exit flow(*)		
y_8	CO-PrOx exit temperature	u_8	HTS exit flow(*)		
y_9	Molar ratio O_2/CO	u_9	LTS exit flow(*)		
y_{10}	Burner exit molar flow	u_{10}	CO-PrOx exit flow(*)		
y_{11}	CO-PrOx CO exit concentration	u_{11}	Bio-ethanol flow(*)		
y_{12}	Net power				
y_{13}	Oxygen excess				
y_{14}	Stack voltage				
y_{15}	ESR pressure(*)				
y_{16}	HTS pressure(*)				
y_{17}	LTS pressure(*)				
y_{18}	CO-PrOx pressure(*)				
y_{19}	H_2 production rate(*)				

Table 3 – Exhaustive search results.

	Sensor locations														SSD
	y_1	y_2	y_3	y_4	y_5	y_6	y_7	y_8	y_9	y_{10}	y_{11}	y_{12}	y_{13}	y_{14}	
C_1	1	0	1	0	0	0	0	1	1	1	0	0	1	0	7.56
C_2	1	1	1	0	0	0	0	1	1	0	0	0	1	0	9.31
C_3	1	0	1	0	0	0	0	1	1	1	0	0	0	1	9.99
C_4	0	0	1	0	0	1	0	1	1	1	0	0	1	0	10.27
C_5	1	1	1	0	0	0	0	1	1	0	0	0	0	1	11.78

- y_{10}: Burner exit molar flow
- y_{13}: Oxygen excess in the FC

A first attempt to propose a decentralized plant-wide control policy is the well-known RGA approach. The RGA (and its variants) allows to define the input–output pairing by using steady-state information, the results are shown in Table 4, where the highlighted values represent a suitable input–output pairing with the following control loops: 1, $y_9 - u_1$; 2, $y_1 - u_2$; 3, $y_3 - u_3$; 4, $y_{10} - u_4$; 5, $y_8 - u_5$ and 6, $y_{13} - u_6$. They configure a decentralized structure.

The standard driving cycles given in Section 3.1.1 are used to evaluate dynamically the plant-wide control proposed in Table 4. The control policy is tested under the urban dynamometer driving schedule cycle because it is considered the most exigent one. For this test, a connection between the dynamic model and the program ADVISOR was performed. The current profile demanded to the fuel cell is presented in Fig. 4(b). The energy management strategy presented in Section 3.2 is applied, where the power distribution is made according with the power demands and the state of energy of the energy storage system.

The synthesized control structure is implemented via unitary output feedback with PI (proportional/integral) controllers. The classical internal model control theory is used for tuning purposes. Table 5 summarizes the selected parameters for each loop, following the guide given in [21]. In Fig. 5 can be seen the proposed control structure since the loops are highlighted with a background. It must be noticed that in control loops 1 and 6 the controlled variable is the ratio between two flows. The first loop uses a molar ratio between O_2 and CO and the second one uses a relationship between both inlet and used oxygen flow in the PEMFC. The load current stack can be applied to estimate the used oxygen flow.

To illustrate the effectiveness of the proposed control strategy a complete set of simulations are given under the UDDS cycle. Fig. 6(a)–(f) summarizes the CV dynamic evolutions for each control loop in the process. In addition, Fig. 7 shows the hydrogen production rate profile and the bioethanol flow response.

Table 4 – RGA for the BPS + FC process.

	u_1	u_2	u_3	u_4	u_5	u_6
y_1	0.0001	**0.9908**	0.0074	0.0014	0.0004	0.0000
y_3	0.0242	0.0012	**0.8882**	0.0844	0.0020	0.0000
y_8	0.3953	0.0011	0.0143	0.0108	**0.5796**	−0.0011
y_9	**0.5776**	0.0005	0.0004	0.0027	0.4187	0.0000
y_{10}	0.0031	0.0064	0.0897	**0.9008**	0.0000	0.0000
y_{13}	−0.0003	0.0000	0.0000	−0.0000	−0.0007	**1.0011**

Bold elements indicate the input-output pairing selected.

Table 5 – Controllers tuning.

	Loop 1	Loop 2	Loop 3	Loop 4	Loop 5	Loop 6
k_c	0.005	0.039	4.5×10^{-5}	0.001	1×10^{-6}	5.071
τ_i^c	2.671	3.327	0.055	0.047	0.05	0.140

Fig. 6(a) shows the dynamic behavior of the control loop no. 1. In this case the CO-PrOx molar ratio O_2/CO (CV) is shown. In Fig. 6(b) can be observed the loop no. 2. In this case the ESR exit temperature as CV is presented. The dynamic response of the control loop no. 3 is shown in Fig. 6(c). Here, the burner exit temperature is the CV. Fig. 6(d) and (e) summarizes the temporal evolution of the control loops number 4 and 5 respectively. The former case deserves a particular explanation because it has a changing reference (working point). In this case is shown the burner exit flow as CV.

According to the disturbance profile some set point modifications must be done. The process was designed for working at a specific current load demand, if that current decreases, the lower hydrogen demand decreases the flow through the ESR. If this situation happens, and the flow of hot gasses passing through the jacket of the reformer are kept constant, the temperature controller reduces the fraction of heat transferred to the main stream, and it will turn out in useful heat loss and consequent decaying of the efficiency of the system. So, to avoid the performance loss, a cascaded set point is established for the flow of gases going out of the burner, that varies according to the demand corresponding with:

$$F_{BRN} = 0.001945 \times I_{st} + 0.007867 \tag{14}$$

where F_{BRN} is the reference to the burner exit flow, that has to be followed manipulating the entering flow of air (oxygen). In Fig. 6(e), the dynamic response of the control loop number 5 is shown where the CO-PrOx exit temperature is the CV.

The dynamic behavior of loop no. 6 is shown in Fig. 6(f), it is the loop that corresponds to the fuel cell. The only variable that can be manipulated is the voltage to the compressor motor, and the considered controlled variable is the oxygen excess in the cathode. To control the amount of air injected to the fuel cell, the compressor motor voltage is adjusted, if it is too little, then the fuel reaction will be incomplete, and that will lead to a low hydrogen utilization. If the amount of oxygen is excessive, a complete reaction will be produced, but the air compressor requires more power, producing a significant decrease of the net efficiency of the system. So, there exists an optimal flow of oxygen for each current load demand, it can be translated in a specific voltage to the compressor. According to the recommendations given in [22], the optimal excess of oxygen, depending of the current demands, is represented by the following equation:

$$\lambda_{O_2}^{exc} = 5.89873e-05 \times I_{st}^2 - 1.79862e-02 \times I_{st} + 4.78035 \tag{15}$$

The production rate control loop is presented in Fig. 7. It has a changing set point, because the hydrogen demand of the

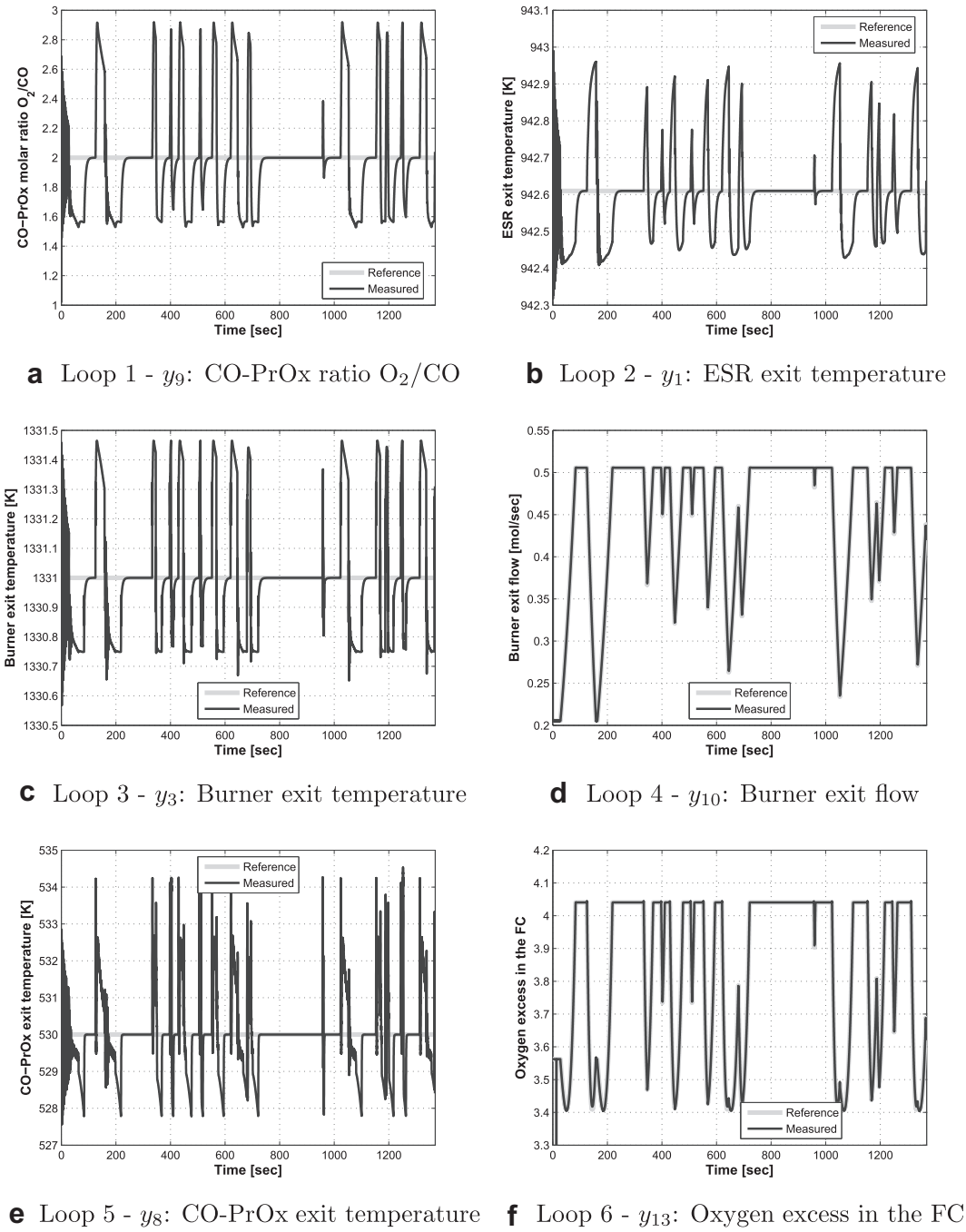

a Loop 1 - y_9: CO-PrOx ratio O_2/CO

b Loop 2 - y_1: ESR exit temperature

c Loop 3 - y_3: Burner exit temperature

d Loop 4 - y_{10}: Burner exit flow

e Loop 5 - y_8: CO-PrOx exit temperature

f Loop 6 - y_{13}: Oxygen excess in the FC

Fig. 6 – Dynamic responses for control loops.

fuel cell varies in accordance with the demanded current as it was described in [22]:

$$W_{H_2} = \frac{n \cdot I_{st}}{2 \cdot F} \tag{16}$$

where W_{H_2} refers to H_2 production (taken as set point), n is the number of cells in the stack and F the Faraday constant. This loop is extremely important for the control objectives of the plant.

In Fig. 8 is shown the distribution of energy among the power sources through the driving cycle. It represents the power demand of the hybrid vehicle, and the distribution of energy to fulfill that specific requirement between the fuel cell and the supercapacitors. When the demand is greater than the power that can be obtained from the fuel cell, it works at its maximum point, and the remaining power is supplied by the ESS. When the demanded energy is low, the fuel cell goes to its minimum, and the excess of the generated power is used to refill the energy of the ESS. In addition, the fuel cell has rate limitations, so when the power change is too sudden, the supercapacitors have to supply the power in order to keep up to the transient demand variation of the system. Analyzing

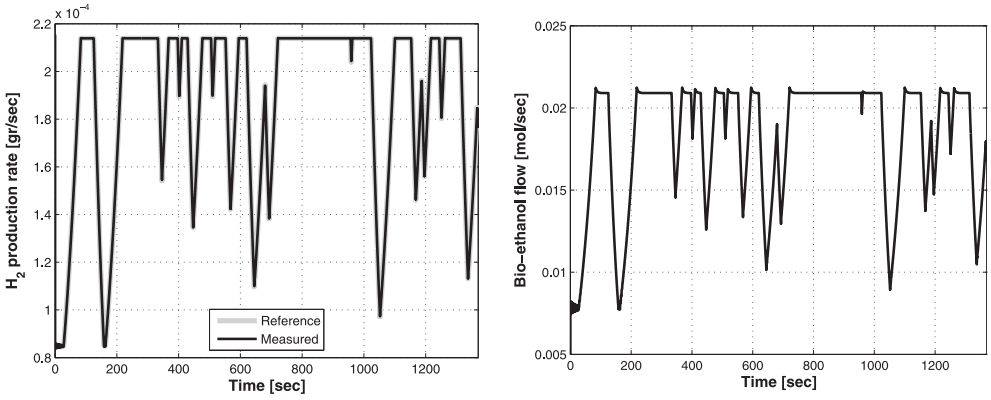

a y_{19}: H_2 production rate **b** u_{11}: Bio-ethanol flow

Fig. 7 – Production rate loop dynamic response.

the behavior of the SoE of the supercapacitors a clear tendency to a decreasing SoE is observed, so a slightly bigger fuel cell could present better performance. Hence, the variability of the energy of the capacitors is very small, indicating that they could be oversized, so less supercapacitors can be enough for the system, decreasing the weight of the vehicle.

A noticeable result is obtained when the moles of fresh ethanol used to fulfill the requirements of the BPS within the considered driving cycle are compared between the different systems considered. The consumption considering a vehicle provided only with the fuel cell is around 26 moles. It has to be considered that the FC actually can not reach the maximum power requirement, so power provided is not enough for the cycle during the peaks of the demand and it is not working in the desired condition. The consumption of ethanol for the hybrid vehicle as described above, presents a 16% reduction in fuel needs, and it can provide the necessary power. When demanded power is higher than the FC capability, the supercapacitors provide the remaining. The theoretical case when the system is working always in maximum efficiency, and fuel consumption is reduced to its minimum, represents a 33% reduction in moles of ethanol.

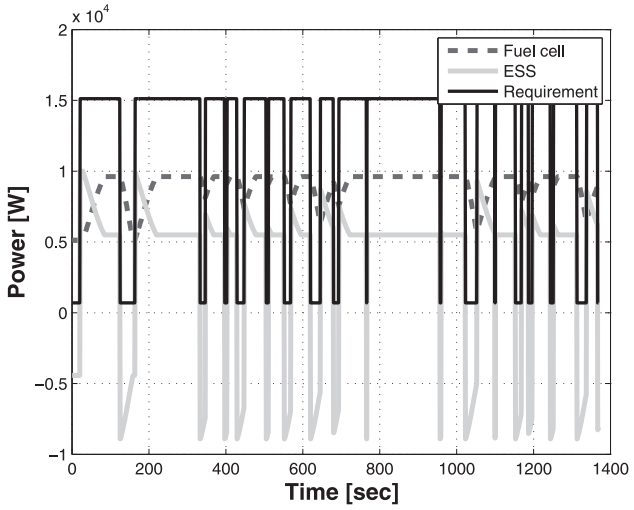

Fig. 8 – Energy distribution between the power sources.

The final part of the procedure shown in Fig. 1 is followed. Taking into account the strategy defined in Section 2.3 the control structure design can be analyzed using the net load effect (NLE) concept. It is done considering the possible contribution that the interaction effect can give between several control loops for rejecting specific disturbances of the process. The problem can be solved as an optimization, considering the minimization of the functional cost of Eq. (10). The combinatorial size results $2^{6\times5} \approx 1.0737 \times 10^9$ for which an exhaustive search is impractical and can be efficiently solved using the model parametrization in Eq. (9), by Genetic Algorithms.

$$\Gamma_o = \begin{bmatrix} 1 & 0 & 1 & 0 & 0 & 1 \\ 1 & 1 & 1 & 1 & 0 & 1 \\ 0 & 0 & 1 & 1 & 1 & 0 \\ 1 & 0 & 1 & 1 & 1 & 0 \\ 1 & 1 & 0 & 0 & 1 & 1 \\ 1 & 0 & 1 & 1 & 0 & 1 \end{bmatrix} \tag{17}$$

The best model parametrization from both the location and amount of its components point of view is shown in Eq. (17), it represents the optimal solution. The GA selects 17 additional components (control loops) according to the array given in Γ_o. In other words, there is no solution with fewer or more components that minimizes the functional cost. Even a solution with the same amount of loops (=17) but different locations of that shown in Γ_o, is suboptimal.

The solution C^4_{NLE} was selected due to a good trade-off between the number of control loops and fitness degradation. If fewer loops are considered the solutions move toward the diagonal structure degrading their NLE index. C^4_{NLE} represents an NLE decrease of ≈9.7% respect to the optimal case, but using only four additional control loops. On the other hand, C^{30}_{NLE} degrades the functional cost in ≈97.2% and uses 30 additional control loops. Finally, C^0_{NLE} degrades the functional cost in ≈130.5% respect to the optimal value but without using additional control loops. Both diagonal and full control structures represent the worst solutions in terms of the NLE index as can be seen in Fig. 9 including the optimal, diagonal,

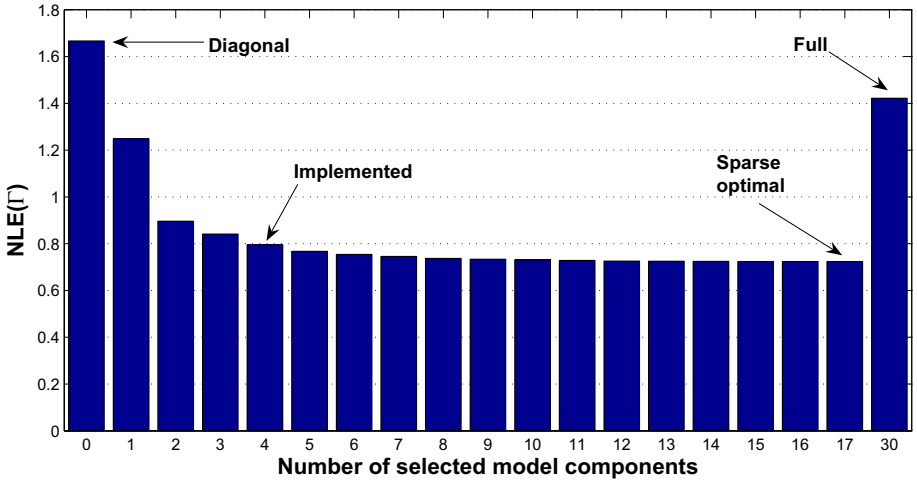

Fig. 9 – NLE index profile for suboptimal solutions.

full and the implemented controller structure ($\mathbf{C}^4_{NLE}$) as solutions.

The sparse (suboptimal) control structure was implemented and evaluated against the diagonal structure. Table 6 presents the Integral Absolute Error (IAE) of the variables with respect to their corresponding references. The control energy is almost the same for both cases, meaning there is no extra effort for the sparse case. However, the value of the IAE index is smaller in most control loops, so it represents a better control structure for a very sensitive plant.

The sparse controller structure implemented actually represents a suboptimal solution to the control problem, so the obtained results are very encouraging. It is a solution that reaches excellent performance without excessive control loops for rejecting disturbances and using the interaction effects.

Both structures require nearly the same amount of control energy. This situation denotes that the plant is extremely sensitive, given that slight modifications in the manipulated variables produce remarkable changes in the controlled ones. The new sparse control structure does not modify the bio-ethanol consumption of the system. It is a satisfactory result, given that, with the same amount of fuel consumed, a better set point tracking is achieved for the changing reference of the hydrogen requirements.

Table 6 – IAE index – UDDS conditions.

Loop no.	CV	Decentralized	Sparse
1	y_9	338.67	324.23
2	y_1	113	89
3	y_3	188.61	58.09
4	y_{10}	1.127	1.126
5	y_6	859.50	1803
6	y_1	6.28	6.03
H_2	y_{14}	2.38e−4	2.30e−4

4. Conclusions

In this work a generalized methodology for plant-wide control design is applied, step-by-step, on the bio-ethanol processor for hydrogen production connected with a PEM fuel cell. The approach needs steady-state process information and identification techniques for obtaining a reduced and linearized model. As a result, the best selection of the controlled variables and a well-conditioned pairing with manipulated variables can be achieved based on the sum of square deviations and the net load effect indexes. The control structure is proposed for achieving the main objectives of quality and efficiency. The methodology allows to sort the objectives according to their inherent importance by means of the weighting matrices selection. For testing the dynamic behavior of the controlled plant, the PEMFC is connected to an automobile motor which is required to respond to the exigences of a standard urban driving cycle, named UDDS. Hence, a complex load profile is generated which constitutes a realistic scenario. For the particular case addressed here, the BPS, 14 CVs are able to be chosen and 6 MVs are available, the selection was performed among 3003 potential solutions. Six optimal CVs were selected, able to minimize the SSD index and using the RGA criteria, a decentralized (diagonal) control structure was proposed. It was mainly dedicated to solve servo problem of the plant. All the control loops have presented a suitable dynamic behavior, with fast correction and little variation from their reference values. They were set as functions of the load demanded. Those variables such as references of the hydrogen production and burner exit flow, have presented good servo performance. On the other hand, loops with fixed set points (temperatures, compositions, flow ratios) have shown good regulating responses. All of these properties have been evaluated through the integral absolute error and variability percentage. The final control structure was obtained by applying the NLE approach giving as a result a sparse controller design. Initially, a complete analysis was developed considering a combinatorial problem of $\approx 1 \times 10^9$

dimension which was solved using genetic algorithms. The optimal solution called $\mathbf{C}_{NLE}^{17}$ proposes to select 17 model components to be accounted for designing the multivariable controller. However, analyzing the other suboptimal solutions, a sparse control structure, with only four model components, was found suitable. It was finally chosen because it involved a controller structure with less off-diagonal elements ($\mathbf{C}_{NLE}^{4}$). This solution presented a best trade-off between the hardware requirements associated with the number of extra control loops and NLE degradation respect to the optimal option. In the last part of this work a complete dynamic evaluation was presented comparing this suboptimal sparse control structure and the decentralized one obtained previously. The achieved improvements by this sparse approach were quantified using integral absolute errors for tracking reference and the control energy involved in each control policy. The sparse control showed a better dynamic performance than the decentralized one. This result suggests that the optimal solution $\mathbf{C}_{NLE}^{17}$ could be able to improve even more the performance given by the option $\mathbf{C}_{NLE}^{4}$ but with higher investment cost.

REFERENCES

[1] Larminie J, Dicks A. In: Fuel cell systems explained. 2nd ed. Wiley and Sons; 2003.

[2] Gregorini VA, Pasquevich D, Laborde M. Price determination for hydrogen produced from bio-ethanol in argentina. International Journal of Hydrogen Energy 2010;35(11):5844–8.

[3] Oliva DG, Francesconi JA, Mussati MC, Aguirre PA. Modeling, synthesis and optimization of heat exchanger networks. application to fuel processing systems for PEM fuel cells. International Journal of Hydrogen Energy 2011;36(15): 9098–114.

[4] Bristol E. On a new measure of interaction for multivariable process control. IEEE Transactions on Automatic Control 1966;11(1):133–4.

[5] Chang J, Yu C. The relative gain for non-square multivariable systems. Chemical Engineering Science 1990;45:1309–23.

[6] Chang J, Yu C. Relative disturbance gain array. AIChE Journal 1992;38:521–34.

[7] He MJ, Cai WJ, Ni W, Xie LH. Rnga based control system configuration for multivariable processes. J. Proc. Control 2009;19:1036–42.

[8] Molina G, Zumoffen D, Basualdo M. A new systematic approach to find plantwide control structures. Computer Aided Chemical Engineering 2009;27:1599–604.

[9] Zumoffen D, Basualdo M. Optimal sensor location for chemical process accounting the best control configuration. Computer Aided Chemical Engineering 2009;27:1593–8.

[10] Molina G, Zumoffen D, Basualdo M. Plant-wide control strategy applied to the tennessee eastman process at two operating points. Computers & Chemical Engineering 2011; 35(10):2081–97.

[11] Arkun Y, Downs J. A general method to calculate input–output gains and the relative gain array for integrating processes. Computers & Chemical Engineering 1990;14:1101–10.

[12] McAvoy T. A methodology for screening level control structures in plantwide control systems. Computers & Chemical Engineering 1998;22:1543–52.

[13] Garcia C, Morari M. Internal model control. 2. Design procedure for multivariable systems. Industrial and Engineering Chemistry Process Design and Development 1985;24:472–84.

[14] Grosdidier P, Morari M, Holt B. Closed-loop properties from steady-state gain information. Industrial and Engineering Chemistry Fundamentals 1985;24:221–35.

[15] Kariwala V. Multi-loop controller synthesis and performance analysis. Ph.D. thesis, University of Alberta, Canada; 2004.

[16] Goodwin G, Graebe S, Salgado M. Control system design. Prentice Hall; 2000.

[17] Skogestad S, Postlethwaite I. Multivariable feedback control. Analysis and design. John Wiley & Sons; 2005.

[18] Nieto Degliuomini L, Biset S, Luppi P, Basualdo M. A rigorous computational model for hydrogen production from bio-ethanol to feed a fuel cell stack. International Journal of Hydrogen Energy 2012;37(4):3108–29.

[19] Markel T, Brooker A, Hendricks T, Johnson V, Kelly K, Kramer B, et al. Advisor: a system analysis tool for advanced vehicle modeling. Journal of Power Sources 2002;110:255–66.

[20] Nieto L, Zumoffen D, Feroldi D, Basualdo M. Dynamic modeling and control of a fuel cell hybrid vehicle with onboard fuel processor. In: Kothare Mayuresh, Tade Moses, Vande Wouwer Alain, Smets Ilse, editors. Proceedings of the 9th international symposium on dynamics and control of process systems. Leuven, Belgium: IFAC; 2010. p. 551–6.

[21] Rivera D. Una metodología para la identificacion integrada con el diseño de controladores IMC-PID. RIAI (Rev. Iberoamericana de Autom e Inf. Ind) 2007;4(4):5–18.

[22] Pukrushpan J, Stefanopoulou A, Peng H. Control of fuel cell power systems: principles, modeling, analysis and feedback design. Springer; 2004.